

The Exploitation of *Aloe saponaria* (syn. *Aloe maculata*) as a Potential Green Corrosion Inhibitor for Bronze in a Neutral Chloride Environment

Bouchra Benzidia ^{1,*}, Mohammed Barbouchi ², Hind Hammouch ¹, Hamid Erramli ¹, Najat Hajjaji ¹

¹ Laboratory of Organic Chemistry, Catalysis, and Environment, Department of Chemistry, Faculty of Sciences, Ibn Tofail University, BP 133, 14000 Kenitra, Morocco; benzidia1511@gmail.com (B.B.); hamhind@yahoo.fr (H.H.); hamid.erramli@uit.ac.ma (H.E.); n_hajjaji@yahoo.fr (N.H.);

² Laboratory of Molecular Chemistry and Natural Substances, Department of Chemistry, Faculty of Sciences, Moulay Ismail University, B.P 11201 Zitoune, Meknes-Morocco; med.barbouchi@gmail.com (M.B.);

* Correspondence: benzidia1511@gmail.com (B.B.);

Scopus Author ID 57201803424 (B.B.)

Received: 26.07.2022; Accepted: 3.10.2022; Published: 19.12.2022

Abstract: The work presented in this article contributes to the valorization of the *Aloe saponaria* (syn. *Aloe maculata*) by evaluating anticorrosive activity. To do this, we first developed a new, simpler, and less expensive method of extraction of *Aloe saponaria* mucilage (ASM). The corrosion inhibition of bronze B66 in 3% NaCl was performed by gravimetric and electrochemical measurements (stationary and transient). Surface analyses complemented this; scanning electron microscopy (SEM) coupled with energy-dispersive X-ray spectroscopy (EDX) provided evidence of the protective power of our inhibitor. Electrochemical measurements matched the results of gravimetric measurements, and we note that our inhibitor's effect modifies the electrochemical process's mechanism at the bronze/3% NaCl interface. In addition, potentiodynamic polarization curves indicated that ASM behaves as a cathodic inhibitor. The inhibition efficiency of ASM is about 88% for a concentration of 750 ppm. The surface investigation by the SEM/EDX confirmed that the corrosion barrier is due to the adsorption of ASM molecules over the bronze/3% NaCl interface.

Keywords: *Aloe saponaria*; anticorrosive activity; bronze B66; 3% NaCl.

© 2022 by the authors. This article is an open-access article distributed under the terms and conditions of the Creative Commons Attribution (CC BY) license (<https://creativecommons.org/licenses/by/4.0/>).

1. Introduction

Corrosion is the deterioration of the original state of the metal under the influence of aggressive media (highly corrosive mineral acids, alkaline and/or saline solutions), which can lead to the destruction of the metal; this is an important economic and industrial problem [1, 2]. Therefore, choosing appropriate corrosion control measures becomes crucial [1]. Several methods have been developed to solve this problem, including corrosion inhibitors. Corrosion inhibitors are one of the most practical methods of corrosion protection in aggressive environments [3].

Most corrosion inhibitors are organic compounds that have attracted great attention due to their high corrosion inhibition efficiency [4, 5]. However, these traditional organic compounds are usually environmentally toxic and non-biodegradable [6]. In recent years, research has focused on the anticorrosive properties of biopolymers [7–12] and natural plant products friendly to the environment [13].

Plant extracts are one such alternative that can be used as an environmentally friendly alternative. The literature review showed that many extracts of plant parts, including bark, leaves, fruits, seeds, roots, twigs, flowers, and even whole plant extracts, are widely used as corrosion inhibitors [14–22].

These natural products contain phytochemicals rich in heteroatoms, namely N, O, P, and S, and electron-rich multiple bonds. The inhibition efficiency of these compounds can be measured as a function of the number of mobile electrons present, the character of the orbital containing the free electrons, and the electron density on the heteroatoms [18, 23].

Nowadays, actual, practical interest in the use of aloe has been increasing. *Aloe vera* L. is a perennial, evergreen herb that thrives primarily in tropical and subtropical climates. It contains large contents of polysaccharides, aloin, different essential minerals, amino acids, vitamins, and other active compounds. Therefore, *Aloe* species have been applied for thousands of years globally as a classic medicinal herb, as well as in cosmetic repair and health care. Among the primary *Aloe* species are *Aloe vera* and *Aloe saponaria* L., which is often known as African *Aloe*, soap *Aloe*, or zebra *Aloe*, and is an arid-zone plant endemic to eastern South Africa, Botswana, and Zimbabwe [24]. *Aloe saponaria* reportedly has antioxidant and anti-inflammatory activities [25]. *Aloe saponaria* possesses antioxidant capacity, antiradical activity, and lipid peroxidation inactivation activity and contains a maximum amount of phenols and flavonoids [24].

Since ancient times, bronzes have been widely used as a valuable human cultural heritage in various fields, such as battery connectors, archaeological objects, urban statues, and sculptures [26, 27]. Bronzes are copper-tin alloys and are formed primarily of copper, usually with 12-12.5% tin and other metals [28].

The bronzes uncovered carry important historical information and are of great interest to archaeological research [27]. Bronze objects are vulnerable to corrosion environments and inevitably suffer varying degrees of corrosion damage due to the existence of moisture and other corrosive fractions, e.g., acid rain containing sulfates, carbonates in the urban and industrial environment, and to chlorides in the marine environment, which are the main cause of "bronze corrosion" [27, 29].

Chloride ions and sulfur compounds are the most common and important atmospheric corrosive agents, as reported [29].

In this study, the reason for using the 3 wt% NaCl medium is to simulate the conditions in seawater characterized by high humidity [30]. Indeed, the concentration of Cl is between 3% and 3.5%; chloride ions are among the most abundant and aggressive corrosive media [31].

Therefore, the objective of the present study was to investigate a new bronze corrosion inhibitor; non-toxic, easy to implement, inexpensive, stable, and reversible. For that purpose, we will examine the inhibitory effect of *Aloe saponaria* mucilage (ASM) to protect bronze B66 in a neutral chloride media. The study was carried out by coupling gravimetric and electrochemical methods. The surface analysis of the bronze samples studied was followed by the SEM coupled to the EDX, highlighting the inhibitors' protective effect.

2. Materials and Methods

2.1. Working electrode.

The material used as a working electrode is bronze B66. The sample of bronze B66, cut using a chainsaw in a cylindrical shape with a diameter of 1cm², was subsequently welded to a

conductor wire and then coated in a thermosetting resin. The coating is made in a plastic mold. This mold is exposed to ambient air for 24 hrs to allow the resin to solidify.

To obtain reliable and reproducible results, the working electrode undergoes, before each test, a pretreatment which consists in polishing its surface with the abrasive papers of silicon carbide of decreasing fineness in grains (600, 800, 1200, 2000). The polishing is then followed by degreasing with acetone then with distilled water, followed by drying before each test.

2.2. Corrosive solution and inhibitor.

The corrosive solution used in this study is a solution of sodium chloride (30 g/L) prepared by dissolving NaCl in distilled water.

The inhibitor used is the *Aloe saponaria* mucilage (ASM), extracted by a new process [32].

2.3. Gravimetric methods.

The gravimetric study (measuring mass loss) is widely used because it is simple and does not require significant equipment. The corrosion rate W ($\text{g}\cdot\text{cm}^{-2}\cdot\text{h}^{-1}$) is calculated by the following Equation 1:

$$w = \left[\frac{m_i - m_f}{S \cdot t} \right] \quad (1)$$

The inhibition efficiency (η_{WL} (%)) was calculated by Equation 2:

$$\eta_{WL}(\%) = \left[\frac{W^\circ - W}{W^\circ} \right] \times 100 \quad (2)$$

where S : the surface of the part (cm^2); t : time (hour); m_i : weighing of the initial weight; m_f : mass after test; W° , and W are the corrosion rates of the sample after immersion in the solution without and with inhibitor, respectively.

2.4. Electrochemical methods.

Electrochemical measurements were obtained using a three-electrode setup; a platinum electrode was used as a counter electrode, an XR300/XR310 Ag/AgCl reference electrode, and the working electrode which is made of bronze B66 with a cylindrical shape (1cm^2 surface).

The measurements were carried out in potentiodynamic mode using a potentiostat/galvanostat SP-200 type "Bio-logic Science instruments". The working electrode was immersed at the corrosion-free potential for one hour. Using the EC-Lab software, the electrochemical parameters were determined from the polarization curves and the electrochemical impedance diagrams.

2.5. SEM/EDX surface analysis techniques.

This technique is based on the analysis of X-ray images emitted by a sample bombarded by the incident electron beam. It allows the qualitative characterization of the composition of the products present in the metal. The EDX analysis is directly related to the atomic number of the element that emits it. In our work, the morphological characterization of the surface of the bronze coupons was carried out at Moroccan Foundation for Advanced Science, Innovation, and Research (MAScIR), by a field emission scanning electron microscope (SEM) and by

energy dispersal. The EDX (X-flash model 6/30 from Bruker) is performed by FEI microscopy (quanta model FEG 450).

3. Results and Discussion

3.1. Gravimetric study.

The values of corrosion rate (g/h.cm^2) and percentage of inhibition efficiency determined by gravimetric method at different concentrations of ASM after 24 hrs of immersion are presented in Table 1.

From this table, it can be seen that the corrosion rate decreases with increasing concentration of the inhibitor in solution; it reaches a value of $4.02 \times 10^{-6} \text{ g/h.cm}^2$ for a concentration of 750 ppm, corresponding to an efficiency of 89.13%. In order to complete these results, we used electrochemical techniques, which are more accurate for the determination of the corrosion rate and the explanation of the influence of our inhibitor on the mechanisms of the corrosion process of bronze B66.

Table 1. Corrosion rate and inhibition efficiency as a function of inhibitor concentrations.

	W (g/h.cm^2)	η_{WL} (%)
3% NaCl	3.70×10^{-5}	-----
250 ppm	1.59×10^{-5}	57.02
500 ppm	1.25×10^{-5}	66.21
750 ppm	4.02×10^{-6}	89.13

3.2. Electrochemical study.

3.2.1. Open circuit potential curves.

Figure 1 represents the variation of the potential, as a function of time, of bronze B66 in 3% NaCl in the absence and presence of ASM at different concentrations.

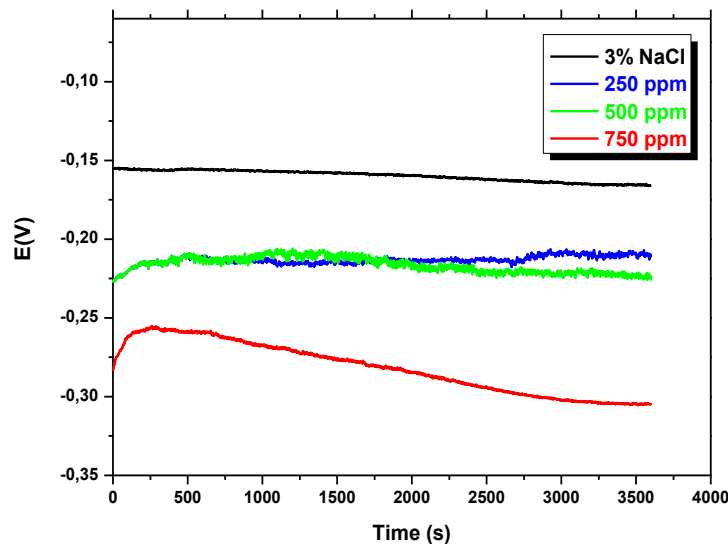


Figure 1. Time evolution of corrosion potential of bronze B66 in 3% NaCl in the presence of ASM at different concentrations.

In the absence of the inhibitor, the corrosion potential of the bronze B66 in 3% NaCl undergoes a variation in the first minutes. After 2500 s, it stabilizes around - 0.165 V. This can be attributed to the formation of a layer of corrosion products on the metal surface [33].

In the presence of the inhibitor, we observed a decrease in the corrosion potential towards negative values for all three concentrations. This evolution of the potential indicates that the inhibitor effect acts preferentially on the cathodic process.

3.2.2. Polarization curves.

The polarization curves are obtained in potentiodynamic mode after one hour of immersion of the bronze B66 electrode in 3% NaCl; the polarization curves in the absence and presence of ASM, at different concentrations, are shown in Figure 2. Thus, the inhibition efficiency (η_{PDP} (%)) was computed by using Equation 3:

$$\eta_{PDP}(\%) = \left[1 - \frac{i_{corr}}{i_{corr}^{\circ}}\right] \times 100 \quad (3)$$

where i_{corr}° and i_{corr} are corrosion current densities values without and with inhibitor, respectively.

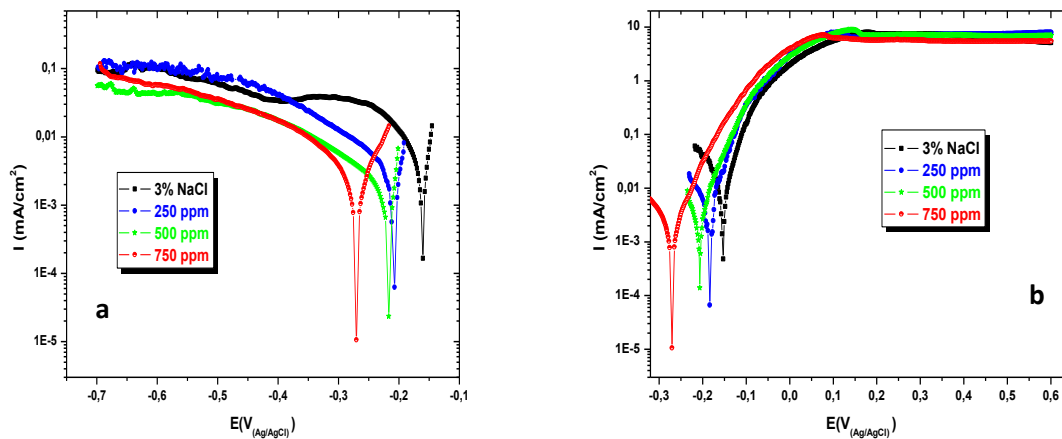


Figure 2. Polarization curves of bronze B66 in 3% NaCl for different ASM concentrations (a) cathodic domain and (b) anodic domain.

In the cathodic domain (Figure 2a), we note that: In the absence of an inhibitor, an increase of the current density in the vicinity of corrosion potential, then it tends to stabilize towards a value of the order of 0.1 mA/cm², corresponding to the limit current of oxygen diffusion [34]. The addition of ASM at different concentrations causes a significant decrease in the current density in the vicinity of E_{corr} . This decrease is more pronounced when the concentration of ASM inhibitor increases, shifting the corrosion potential towards more negative values. For potentials higher than -0.45 V, we notice the appearance of a linear part translating an exponential variation of the current. This range becomes wider when the inhibitor concentration increases.

In the anodic domain (Figure 2b), we notice that: In the absence of an inhibitor, the current density increases rapidly in the vicinity of the corrosion potential, reflecting the oxidation of the material, and then tends to stabilize towards a value in the order of 10 mA/cm², which is too high to signify passivation of the metal. In the presence of the inhibitor, there is a small decrease in the values of the anodic current density, which is less marked compared to the cathodic domain.

Therefore, from these results, it can be seen that the tested compound is a cathodic inhibitor. The electrochemical parameters derived from the polarization curves are shown in Table 2.

Table 2. Electrochemical parameters derived from polarization curves of bronze B66 in 3% NaCl in the absence and presence of ASM.

	$-\beta_e$ (mV)	$-E_{corr}$ (mV _{Ag/AgCl})	I_{corr} (μA/cm ²)	η_{PDP} (%)
3%NaCl	63.4	165.8 ± 3.3	9.48 ± 0.10	-----
250 ppm	50.0	206.2 ± 0.9	1.26 ± 0.01	86.70
500 ppm	51.0	215.5 ± 1.1	1.13 ± 0.01	88.08
750 ppm	51.6	267.1 ± 1.1	0.92 ± 0.01	90.29

From the electrochemical parameters collected in the table, it can be seen that increasing the concentration leads to a decrease in the current density value. The inhibition efficiency reaches 90% for a concentration of 750 ppm inhibitor. The results obtained show that the inhibitor is of cathodic type. It acts in low concentration; its protective effect is translated by forming a film of inhibitor on the metal surface, leading to a decrease in the corrosion current density values [14].

3.2.3. Electrochemical impedance diagrams.

Figure 3 shows the impedance diagrams of bronze B66 in 3% NaCl in the absence and presence of different concentrations of ASM after one hour of immersion. These measurements are performed in a frequency range from 100 KHz to 10 mHz. As regards the inhibition efficiency (η_{EIS} (%)) was computed by Equation 4:

$$\eta_{EIS}(\%) = \left[1 - \frac{R_p}{R_{p(inh)}}\right] \times 100 \tag{4}$$

where the $R_{p(inh)}$ and R_p represent the transfer resistance without and with the addition of an inhibitor, respectively.

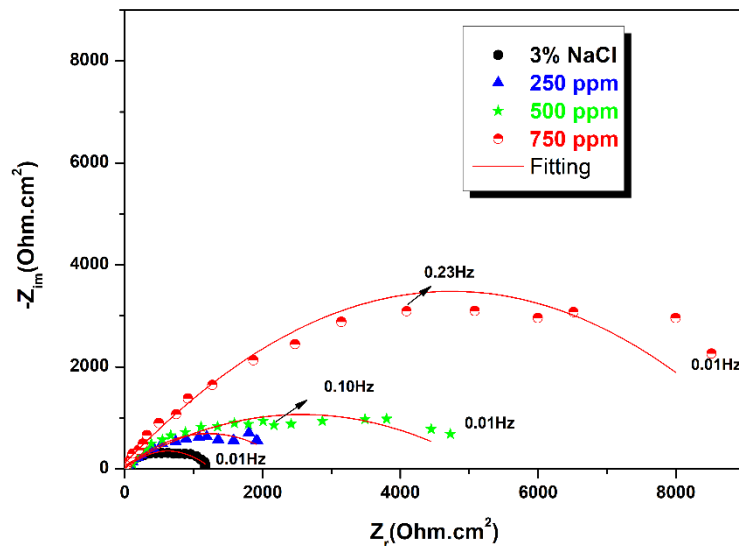


Figure 3. Electrochemical impedance diagrams of bronze B66 in 3% NaCl at different inhibitor concentrations after 1h immersion.

In the absence of an inhibitor, we notice the appearance of two capacitive loops (Figure 3). First, a capacitive loop at high frequencies, attributed to the charge transfer, which controls the interfacial process and whose polarization resistance is about 1143 Ωcm². Dispersion at low frequencies is related to matter transport [26]. The equivalent circuit is composed of two RC circuits in parallel.

The addition of the inhibitor at different concentrations shows the appearance of two capacitive loops with a significant increase in polarization resistance. At high frequencies, the size of the capacitive loop increases with concentration [35]. An equivalent 2RC circuit in parallel can interpret these curves (Figure 4b).

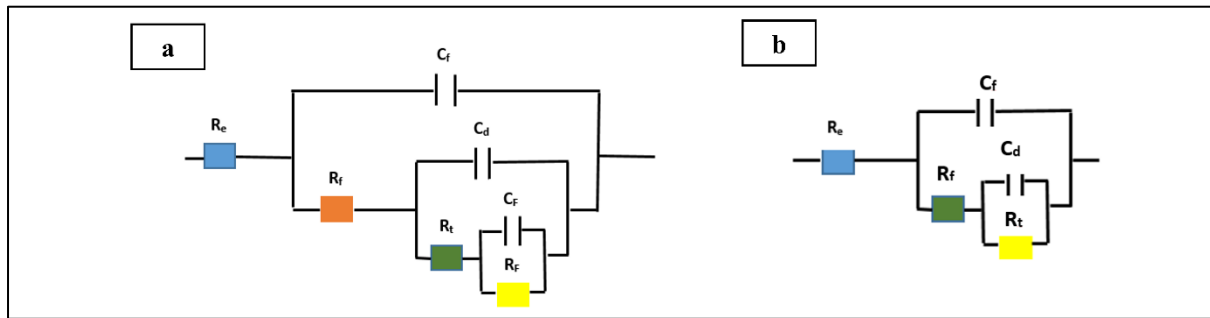


Figure 4. Equivalent electrical circuits of electrochemical impedance diagrams (a) in the absence of ASM and (b) in the presence of ASM.

At high frequencies ($R_f - C_f$), the diameters of the capacitive loops are on the order of $316 \Omega\text{cm}^2$, $325 \Omega\text{cm}^2$, and $970 \Omega\text{cm}^2$ for 250 ppm, 500 ppm, and 750 ppm ASM concentrations, respectively.

The contribution ($R_t - C_d$) at low frequencies is attributed to the double-layer capacitance at the studied interface and the charge transfer resistance. The polarization resistance increases significantly with concentration.

The fitting results of the electrochemical parameters drawn from the electrochemical impedance diagrams in Figure 3 are represented in Table 3.

Table 3. Electrochemical parameters derived from electrochemical impedance diagrams.

	R_e ($\Omega\text{.cm}^2$)	R_f ($\Omega\text{.cm}^2$)	C_f ($\mu\text{F/cm}^2$)	R_t ($\Omega\text{.cm}^2$)	C_d ($\mu\text{F/cm}^2$)	R_p ($\Omega\text{.cm}^2$)	C_F ($\mu\text{F/cm}^2$)	R_p ($\Omega\text{.cm}^2$)	η_{EIS} (%)
3% NaCl	8.91	-----	-----	703	147.9	440	860	1143 ± 22	-----
250 ppm	11.91	316.7	23.27	1150	79.99	-----	-----	1467 ± 07	22.08
500 ppm	11.84	325.0	22.25	5004	72.13	-----	-----	5329 ± 26	78.55
750 ppm	10.75	970.6	20.66	8333	46.67	-----	-----	9304 ± 46	87.71

Table 3 shows that the polarization resistance increases with inhibitor concentration; it increases from $1143 \Omega\text{.cm}^2$ in the absence of an inhibitor to $9304 \Omega\text{.cm}^2$ in the presence of 750 ppm in ASM. The inhibition efficiency increases with the inhibitor concentration and reaches 87.71% for a concentration of 750 ppm in ASM.

3.3. Surface analysis by SEM/EDX.

SEM images coupled with EDX analysis of the metal surface in the absence and presence of 750 ppm ASM after 24 hrs of immersion are shown in Figure 5 and Figure 6.

The results found showed that in the absence of the inhibitor, the appearance of chloride ions causes the degradation of the metal. However, in the presence of ASM, we note the disappearance of chloride ions and the appearance of carbon, which certainly corresponds to the carbon chains of ASM. This confirms the protective effect of the inhibitor tested and the results found from the electrochemical measurements made.

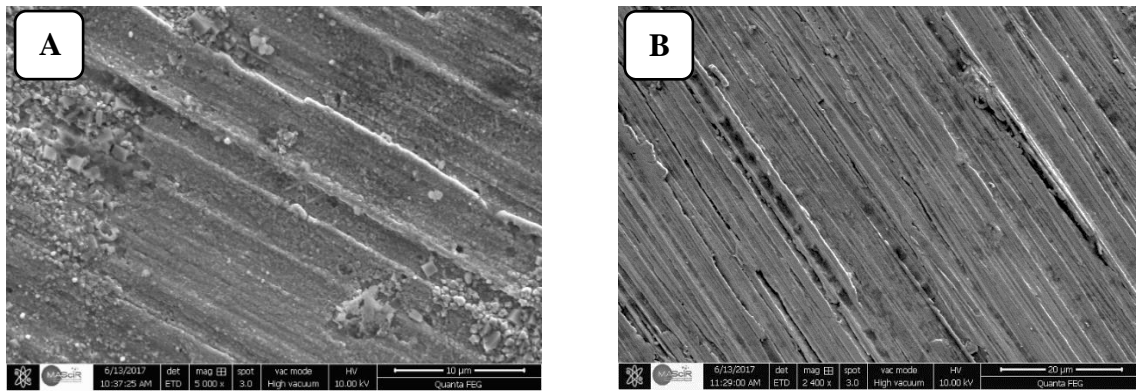


Figure 5. SEM images of bronze B66 after 24 hrs of immersion in a 3% NaCl solution (A) in the absence of ASM and (B) in the presence of 750 ppm ASM.

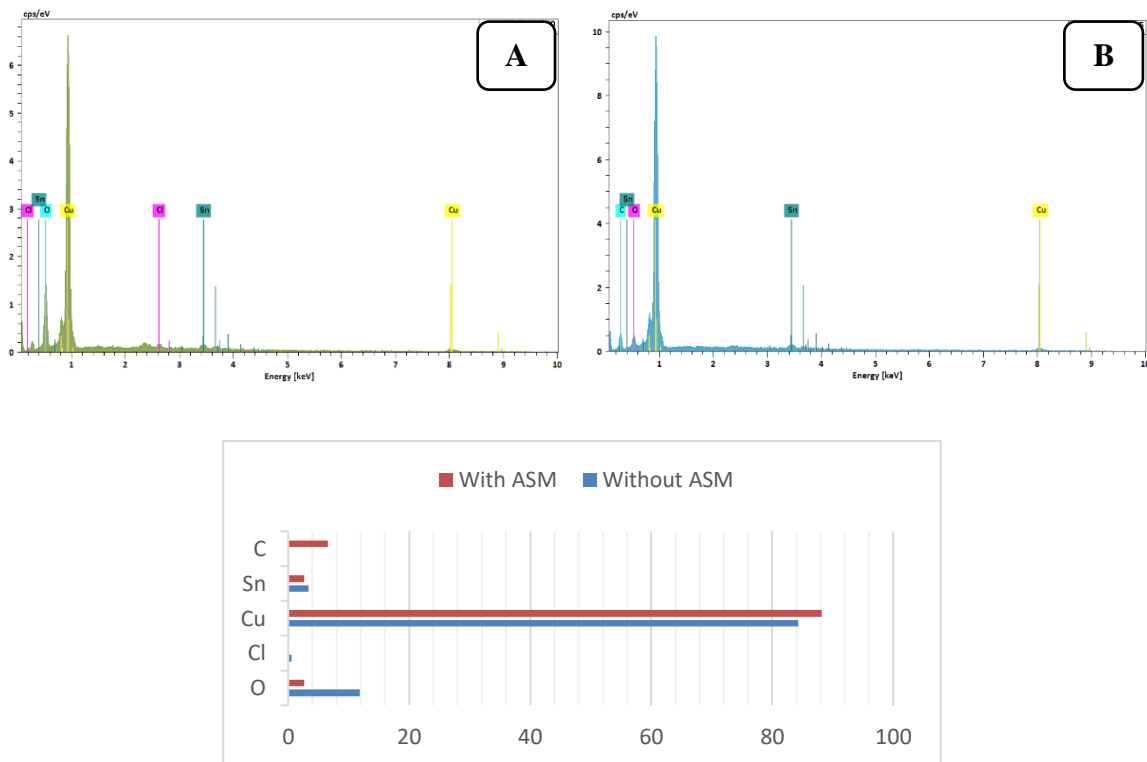


Figure 6. EDX of bronze B66 after 24 hrs of immersion in a 3% NaCl solution (A) in the absence of ASM and (B) in the presence of 750 ppm ASM.

4. Conclusions

Gravimetric and electrochemical methods, stationary (potentiodynamic curves), and transient (electrochemical impedance spectroscopy) evaluated the inhibitory properties of the *Aloe saponaria* mucilage. The results obtained showed that the *Aloe saponaria* mucilage effectively inhibits the corrosion of bronze B66 in 3% NaCl. The inhibition efficiency is about 88% for a concentration of 750 ppm. Furthermore, the surface analysis of the bronze B66 after 24 hrs of immersion in 3% NaCl was performed by SEM/EDX. This analysis clearly shows the substrate's protection in our inhibitor's presence.

Funding

This research received no external funding.

Acknowledgments

This research has no acknowledgment.

Conflicts of Interest

The authors declare no conflict of interest.

References

1. Quraishi, M.A.; Chauhan, D.S.; Saji, V.S. Heterocyclic biomolecules as green corrosion inhibitors. *J. Mol. Liq.* **2021**, *341*, 117265, <https://doi.org/10.1016/j.molliq.2021.117265>.
2. Khanari, K.; Finšgar, M. Organic corrosion inhibitors for aluminum and its alloys in chloride and alkaline solutions: A review. *Arab. J. Chem.* **2019**, *12*, 4646–4663, <https://doi.org/10.1016/j.arabjc.2016.08.009>.
3. Goyal, M.; Kumar, S.; Bahadur, I.; Verma, C.; Ebenso, E.E. Organic corrosion inhibitors for industrial cleaning of ferrous and non-ferrous metals in acidic solutions: A review. *J. Mol. Liq.* **2018**, *256*, 565–573, <https://doi.org/10.1016/j.molliq.2018.02.045>.
4. Liu, Z.Y.; Wang, D.; Li, D.T.; Wang, H.Q. The inhibition efficiencies of some organic corrosion inhibitors of iron: An insight from density functional theory study. *Comput. Theor. Chem.* **2022**, *1214*, 113759, <https://doi.org/10.1016/j.comptc.2022.113759>.
5. Verma, C.; Ebenso, E.E.; Quraishi, M.A. Molecular structural aspects of organic corrosion inhibitors: Influence of –CN and –NO₂ substituents on designing of potential corrosion inhibitors for aqueous media. *J. Mol. Liq.* **2020**, *316*, 113874, <https://doi.org/10.1016/j.molliq.2020.113874>.
6. Zhang, Q.H.; Hou, B.S.; Li, Y.Y.; Lei, Y.; Wang, X.; Liu, H.F.; Zhang, G.A. Two amino acid derivatives as high efficient green inhibitors for the corrosion of carbon steel in CO₂-saturated formation water. *Corros. Sci.* **2021**, *189*, 109596, <https://doi.org/10.1016/j.corsci.2021.109596>.
7. Hsissou, R. Review on epoxy polymers and its composites as a potential anticorrosive coatings for carbon steel in 3.5% NaCl solution: Computational approaches. *J. Mol. Liq.* **2021**, *336*, 116307, <https://doi.org/10.1016/j.molliq.2021.116307>.
8. Hsissou, R.; Azogagh, M.; Benhiba, F. et al. Insight of development of two cured epoxy polymer composite coatings as highly protective efficiency for carbon steel in sodium chloride solution: DFT, RDF, FFV and MD approaches. *J. Mol. Liq.* **2022**, *360*, 119406, <https://doi.org/10.1016/j.molliq.2022.119406>.
9. Hsissou, R.; Benhiba, F.; Echihi, S.; Benzidia, B.; Cherrouf, S.; Haldhar, R.; Ahmad Alvi, P.; Kaya, S.; Serdaroglu, G.; Zarrouk, A. Performance of curing epoxy resin as potential anticorrosive coating for carbon steel in 3.5% NaCl medium: Combining experimental and computational approaches. *Chem. Phys. Lett.* **2021**, *783*, 139081, <https://doi.org/10.1016/j.cplett.2021.139081>.
10. Moaref, R.; Shahini, M.H.; Eivaz Mohammadloo, H.; Ramezanzadeh, B.; Yazdani, S. Application of sustainable polymers for reinforcing bio-corrosion protection of magnesium implants—a review. *Sustain. Chem. Pharm.* **2022**, *29*, 100780, <https://doi.org/10.1016/j.scp.2022.100780>.
11. Singh, A.; Ansari, K.R.; Alanazi, A.K.; Quraishi, M.A.; Ali, I.H.; Lin, Y. Probing inhibition effect of novel biopolymer based composite for the inhibition of P110 steel corrosion in 15% HCl under dynamic condition. *Sustain. Chem. Pharm.* **2022**, *26*, 100599, <https://doi.org/10.1016/j.scp.2022.100599>.
12. Shahini, M.H.; Ramezanzadeh, B.; Mohammadloo, H.E. Recent advances in biopolymers/carbohydrate polymers as effective corrosion inhibitive macro-molecules: A review study from experimental and theoretical views. *J. Mol. Liq.* **2021**, *325*, 115110, <https://doi.org/10.1016/j.molliq.2020.115110>.
13. Alrefaee, S.H.; Rhee, K.Y.; Verma, C.; Quraishi, M.A.; Ebenso, E.E. Challenges and advantages of using plant extract as inhibitors in modern corrosion inhibition systems: Recent advancements. *J. Mol. Liq.* **2021**, *321*, 114666, <https://doi.org/10.1016/j.molliq.2020.114666>.
14. Benzidia, B.; Barbouchi, M.; Hsissou, R.; Zouarhi, M.; Erramli, H.; Hajjaji, N. A combined experimental and theoretical study of green corrosion inhibition of bronze B66 in 3% NaCl solution by *Aloe saponaria* (syn. *Aloe maculata*) tannin extract. *Curr. Res. Green Sustain. Chem.* **2022**, *5*, 100299, <https://doi.org/10.1016/j.crgsc.2022.100299>.
15. Barbouchi, M.; Benzidia, B.; Aouidate, A.; Ghaleb, A.; El Idrissi, M.; Choukrad, M. Theoretical modeling and experimental studies of Terebinth extracts as green corrosion inhibitor for iron in 3 % NaCl medium. *J. King Saud Univ. - Sci.* **2020**, *32*, 2995–3004, <https://doi.org/10.1016/j.jksus.2020.08.004>.

16. Hossain, N.; Chowdhury, M.A.; Iqbal, A.K.M.P.; Ahmed, A.K.M.F.; Islam, M.S. Corrosion behavior of aluminum alloy in NaOH and *Syzygium Samarangense* solution for environmental sustainability. *Curr. Res. Green Sustain. Chem.* **2022**, *5*, 100254, <https://doi.org/10.1016/j.crgsc.2021.100254>.
17. Hossain, N.; Chowdhury, M.A.; Iqbal, A.K.M.P.; Islam, M.S.; Sheikh Omar, N.Y.; Saifullah, A.Z.A. *Paederia Foetida* leaves extract as a green corrosion inhibitor for mild steel in hydrochloric acid solution. *Curr. Res. Green Sustain. Chem.* **2021**, *4*, 100191, <https://doi.org/10.1016/j.crgsc.2021.100191>.
18. Shahmoradi, A.R.; Ranjbarghanei, M.; Javidparvar, A.A.; Guo, L.; Berdimurodov, E.; Ramezanzadeh, B. Theoretical and surface/electrochemical investigations of walnut fruit green husk extract as effective inhibitor for mild-steel corrosion in 1M HCl electrolyte. *J. Mol. Liq.* **2021**, *338*, 116550, <https://doi.org/10.1016/j.molliq.2021.116550>.
19. Hajsafari, N.; Razaghi, Z.; Tabaian, S.H. Electrochemical study and molecular dynamics (MD) simulation of aluminum in the presence of garlic extract as a green inhibitor. *J. Mol. Liq.* **2021**, *336*, 116386, <https://doi.org/10.1016/j.molliq.2021.116386>.
20. Khayatkashani, M.; Soltani, N.; Tavakkoli, N.; Nejatian, A.; Ebrahimian, J.; Mahdi, M.A.; Salavati-Niasari, M. Insight into the corrosion inhibition of *Biebersteinia multifida* root extract for carbon steel in acidic medium. *Sci. Total Environ.* **2022**, *836*, 155527, <https://doi.org/10.1016/j.scitotenv.2022.155527>.
21. Wang, Q.; Liu, L.; Zhang, Q.; Wu, X.; Zheng, H.; Gao, P.; Zeng, G.; Yan, Z.; Sun, Y.; Li, Z.; Li, X. Insight into the anti-corrosion performance of *Artemisia argyi* leaves extract as eco-friendly corrosion inhibitor for carbon steel in HCl medium. *Sustain. Chem. Pharm.* **2022**, *27*, 100710, <https://doi.org/10.1016/j.scp.2022.100710>.
22. Prifiharni, S.; Mashanafie, G.; Priyotomo, G.; Royani, A.; Ridhova, A.; Elya, B.; Soedarsono, J.W. Extract sarampa wood (*Xylocarpus Moluccensis*) as an eco-friendly corrosion inhibitor for mild steel in HCl 1M. *J. Indian Chem. Soc.* **2022**, *99*, 100520, <https://doi.org/10.1016/j.jics.2022.100520>.
23. Yadav, M.; Goel, G.; Hatton, F.L.; Bhagat, M.; Mehta, S.K.; Mishra, R.K.; Bhojak, N. A review on biomass-derived materials and their applications as corrosion inhibitors, catalysts, food and drug delivery agents. *Curr. Res. Green Sustain. Chem.* **2021**, *4*, 100153, <https://doi.org/10.1016/j.crgsc.2021.100153>.
24. Abou-Sreea, A.I.B.; Roby, M.H.H.; Mahdy, H.A.A.; Abdou, N.M.; El-Tahan, A.M.; El-Saadony, M.T.; El-Tarabily, K.A.; El-Saadony, F.M.A. Improvement of Selected Morphological, Physiological, and Biochemical Parameters of Roselle (*Hibiscus sabdariffa* L.) Grown under Different Salinity Levels Using Potassium Silicate and *Aloe saponaria* Extract. *Plants* **2022**, *11*, 497, <https://doi.org/10.3390/plants11040497>.
25. Adetunji, T.L.; Olisah, C.; Adegbaju, O.D.; Olawale, F.; Adetunji, A.E.; Siebert, F.; Siebert, S. The genus *Aloe*: A bibliometric analysis of global research outputs (2001–2020) and summary of recent research reports on its biological activities. *South African J. Bot.* **2022**, *147*, 953–975, <https://doi.org/10.1016/j.sajb.2022.01.030>.
26. Espinoza Vázquez, A.; Figueroa, I.A.; Gómez, F.J.R.; Vásquez, A.P.; Mata, R.; Ángeles Beltrán, D.; Miralrio, A.; Castro, M. (-) - Epicatechin gallate as a corrosion inhibitor for bronze in a saline medium and theoretical study. *J. Mol. Struct.* **2021**, *1227*, 129416, <https://doi.org/10.1016/j.molstruc.2020.129416>.
27. Zhao, L.; Wei, L.; Li, Q. A highly corrosion resistant and nondestructive menthol coating strategy for short-term protection of bronzes. *Prog. Org. Coatings* **2022**, *170*, 106947, <https://doi.org/10.1016/j.porgcoat.2022.106971>.
28. Sankar, J.; Suresh Kumar, S.; Balamurugan, P.; Kumar, S.; Saleem, S.A.; Krishna, S.V. Fabrication and corrosion studies of bronze based composite prepared through powder metallurgy route. *Mater. Today Proc.* **2021**, *50*, 1067–1070, <https://doi.org/10.1016/j.matpr.2021.07.461>.
29. Šatović, D.; Desnica, V.; Fazinić, S.; Mičetić, M. Studies of bronze corrosion phenomena by EBS and complementary techniques. *Nucl. Instruments Methods Phys. Res. Sect. B: Beam Interact. with Mater. Atoms* **2019**, *461*, 154–158, <https://doi.org/10.1016/j.nimb.2019.09.040>.
30. Fernine, Y.; Ech-chihbi, E.; Arrousse, N.; El Hajjaji, F.; Bousraf, F.; Ebn Touhami, M.; Rais, Z.; Taleb, M. *Ocimum basilicum* seeds extract as an environmentally friendly antioxidant and corrosion inhibitor for aluminium alloy 2024 -T3 corrosion in 3 wt% NaCl medium. *Colloids Surfaces A Physicochem. Eng. Asp.* **2021**, *627*, 127232, <https://doi.org/10.1016/j.colsurfa.2021.127232>.
31. Rodríguez-Gómez, F.J.; Valdelamar, M.P.; Vazquez, A.E.; Del Valle Perez, P.; Mata, R.; Miralrio, A.; Castro, M. Mycophenolic acid as a corrosion inhibitor of carbon steel in 3% wt. NaCl solution. An experimental and theoretical study. *J. Mol. Struct.* **2019**, *1183*, 168–181, <https://doi.org/10.1016/j.molstruc.2018.12.035>.

32. Benzidia, B.; Hajjaji, N.; Hammouch, H.; Belahbib, N. Procédé d'extraction de mucilage d'*Aloe Vera* **2018**, MA 39394 B1.
33. Benzidia, B.; Hammouch, H.; Dermaj, A.; Benassaoui, H.; About, S.; Hajjaji, N. Investigation of green corrosion inhibitor based on *Aloe vera* (L.) burm. F. for the protection of bronze B66 in 3% NaCl. *Anal. Bioanal. Electrochem.* **2019**, *11*, 165–177.
34. Rahmouni, K.; Takenouti, H.; Hajjaji, N.; Srhiri, A.; Robbiola, L. Protection of ancient and historic bronzes by triazole derivatives. *Electrochim. Acta* **2009**, *54*, 5206–5215, <https://doi.org/10.1016/j.electacta.2009.02.027>.
35. von Putlitz, G.S.; Vázquez, A.E.; Gómez, F.J.R.; Negrón-Silva, G.E.; Figueroa, I.A.; Orozco-Cruz, R.; Miralrio, A.; Castro, M. Corrosion inhibition of 1-Benzyl-4-((benzyloxy) methyl)-1H-1,2,3-triazole (BBT) for C844 bronze in saline medium and theoretical study. *J. Mol. Struct.* **2022**, *1267*, 133590, <https://doi.org/10.1016/j.molstruc.2022.133590>.